Author/s:
Zhao, L;Lee, PVS;Ackland, DC;Broom, ND;Thambyah, A

Title:
Microstructure Variations in the Soft-Hard Tissue Junction of the Human Anterior Cruciate Ligament

Date:
2017-09-01

Citation:
Zhao, L., Lee, P. V. S., Ackland, D. C., Broom, N. D. & Thambyah, A. (2017). Microstructure Variations in the Soft-Hard Tissue Junction of the Human Anterior Cruciate Ligament. Anatomical Record, 300 (9), pp.1547-1559. https://doi.org/10.1002/ar.23608.

Persistent Link:
https://hdl.handle.net/11343/292872

Microstructure variations in the soft-hard tissue junction of the human anterior cruciate ligament.

Lei Zhao[1], Peter V Lee[2], David C Ackland[2], Neil D Broom[1], Ashvin Thambyah[1]

[1]Experimental Tissue Mechanics Laboratory, Department of Chemical and Materials Engineering, University of Auckland, New Zealand

[2]Department of Mechanical Engineering, University of Melbourne, Victoria, Australia.

Correspondence
Ashvin Thambyah, PhD
Associate Professor
Department of Chemical and Materials Engineering
University of Auckland
Private Bag 92019
Auckland
New Zealand

Tel: +64 9 373 7599 ext 85379
Fax: +64 9 373 7463

ashvin.thambyah@auckland.ac.nz

Running title: Structure Variations of Human ACL Enthesis

ABSTRACT

The role of the sub-bundles in the anterior cruciate ligament (ACL) has been defined, such that the anterior-medial bundle directly resists anterior tibial translation while the posterior lateral bundle is involved in rotational stability. With regards to this biomechanical function, much of the previous work on bundle-specific morphology has been carried out on the macro-scale, with much less attention given to the micro-to-ultrastructural scalar levels. This is especially true of the enthesis and its microstructure, a biomechanically significant region that has been largely neglected in the published literature dealing with ACL sub-bundle anatomy. In this study, the human ACL tibial enthesis was investigated at multiple scalar levels using differential interference contrast (DIC) and scanning electron microscopies with the aim of determining whether the sub-bundle ligament structure, and its known macro-scale function, is consistent with its micro-architecture at the ligament-bone junction. The investigation found that different ligament insertion morphologies exist between the two bundles, where the AM bundle has more intense interdigitation with the bone matrix than that of the PL bundle. The results suggest that such structure-function relationships, especially across scalar-levels, provide new insight into the significance of the sub-bundle anatomy of the ACL.

Key words: Enthesis; interdigitation; AM and PL bundle

INTRODUCTION

The anterior cruciate ligament (ACL) can be divided into two functional bundles, the anteromedial (AM) and posterolateral (PL), where these have been found to be most involved in anterior tibial translation and rotation respectively (Amis, 2012). The double-bundle structure is arguably the most frequently discussed anatomical feature relevant to ACL reconstruction techniques and its related biomechanics (Zantop et al., 2007; Amis, 2012). It has been proposed that reproducing the double-bundle anatomy of the ACL is important for restoring the normal kinematics of the knee post-surgery (Fu and Lin, 2013). However, a recent review of different ACL reconstruction techniques indicates that kinematics is still not returned to normal levels even with restoration of the double bundle configuration (Gadikota et al., 2015). The discrepancy in the outcomes reported in different studies may be due to the still undefined anatomical understanding of the ACL structure and hence provides much motivation for those that still believe the key to post-operation outcome improvement is based on an anatomic ACL reconstruction (Kato et al., 2010; Yasuda et al., 2010; Dai, 2012; Hofbauer et al., 2013). Therefore, the quest to gain further insight into the native ACL functional anatomy continues, and we argue that one crucial aspect that requires further understanding, is how the insertion of the ACL into bone is achieved.

Interestingly, while the AM and PL bundles are so-called, based on their insertion positions in the tibial plateau, very little is known of the entheses in relation to these bundles. Most studies of the bundle entheses have defined their macro-level and topography-related morphology features (Harner et al., 1999; Ferretti et al., 2007; Ferretti et al., 2012). Some have investigated down to the microscale (Steineman et al., 2016) but still have not distinguished between bundles, nor explored further into the sub-micro scalar levels. Fewer studies have

provided rigorous structural detail, rather mostly focussing on compositional changes along the gradual transition of soft-to-hard tissue (Moffat et al., 2008; Beaulieu et al., 2015; Dai et al., 2015). These studies have shown that the femoral attachment has more fibrocartilage than the tibial (Beaulieu et al., 2015), and regional fibrocartilage variations in the tibia suggest a biomechanical rationale for greater load transfer on the medial aspect (Dai et al., 2015). Despite the current literature on the subject, there is still a significant gap in our understanding of the multi-scalar structural anatomy of the ACL entheses with regards to the double bundle-bone integration.

To this end, the authors have utilised multi-scalar imaging, from macro-to-micro-to-nano levels, to gain new insights into the functionally graded continuum of the porcine ACL soft tissue integration into hard bone (Zhao et al., 2014). Such detail of the multiscale structural make-up of the porcine ACL tibial enthesis was reported as the first study of its kind to reveal the insertion of the AM and PL bundles of the ACL into the tibia. In that study, it was found that in the porcine ACL there were three subtypes of enthesis, relating to (1) bundle type (i.e. AM versus PL), (2) position (i.e. medial versus lateral) and (3) function (i.e. resisting axial versus torsional strains). However, given that the limitation of the above study was carried out on porcine ACL, with its known differences to human (Proffen et al., 2012), the aim of this new study is to apply our imaging techniques to investigate the micro-to-ultra structural insertion of the human ACL into the tibial plateau. The results will be used to provide an initial hypothesis on bundle specific structural characteristics of the human ACL at multi-scale levels.

METHODS

Six paired human knee joints from three female donors aged at 89, 90, and 92 were used in the study. Specimens were obtained through the University of Melbourne body donor program, with approval obtained through the institutions Human Ethics Advisory Committee (1238013), and all structural analysis was conducted in the Experimental Tissue Mechanics Laboratory, Department of Chemical and Materials Engineering, University of Auckland. All specimens were visually examined for osteoarthritis, and meniscus and ligament injuries during harvesting, and no sign of gross defects or overt tissue degeneration was found. Each knee was dissected, the ACL ligament-to-tibial bone samples were harvested and formalin fixed, without any constraint, in the ligaments' relaxed orientation relative to its insertion into the tibial plateau (Fig. 1). Although the ACL loses its natural twist after being removed from the knee joint, the full picture of its intrinsic fibre orientation, in the relaxed state, has been captured by formalin fixation. All samples were imaged using macro photography.

Following dissection, samples of the ACL and its tibial insertions were mildly decalcified and then cryo-sectioned to produce sagittal slices (~30μm thick) of the ligament-bone enthesis. The sections were then digitally imaged in their *fully hydrated state* using both light and differential interference contrast (DIC) optical microscopy.

At the ligament-bone junction, cement-line irregularity was quantified via a 'rugosity' measurement. Rugosity was taken as the ratio of the length of the bone cement line of a given span in the micro-image, divided by the straight horizontal distance of that span, a large ratio being indicative of a highly irregular interface compared to a ratio closer to unity. Serial sections amounting to up to (depending on the width of the sample) 180 sections from the medial-most to the lateral-most aspect of the ACL were obtained and placed into well plates according to their

respective positions. In these 180 sections, since there were no easily discernible differences in sections obtained from near to each other, it was deemed expedient to sample with sufficiently large intervals across the entire collection of sections. Thirty sections were thus sampled from these well plates, each taken with sufficient intervals, between 30 to 240 μm, to represent the progressive position-related structural changes from the medial-most to the lateral-most aspect of the ACL. All thirty sections per ACL were imaged and studied. For rugosity measurements, a total of six sections from the thirty imaged sections were used. The imaged sections were firstly labelled from one to thirty in ascending order, from the medial most to the lateral most positions. Then starting from the third section, every fifth section (i.e. sections 3, 8, 13, 18, 23, and 28) was sampled to represent the span of sectioning across the medial to lateral most aspects. If a section was not capturing the full length of the ligament bundle insertion, the closest intact section with the clearest cement line was used instead. To determine the AM and PL bundle in the present samples, we used our insight from an earlier study on porcine ACL (Zhao et al., 2014). In the porcine ACL, the gross or macro-scale morphology of the AM and PL bundles is very distinct (Zhao et al., 2014; Moffat et al., 2008), and can be correlated to micro-images of distinct changes in bone contour and fibre direction at the enthesis. For this study, bone contours and fibre direction changes were used to distinguish between the two bundles. Consequently, rugosity measurements were made relative to these contours, defining the start and end of an AM or PL bundle. The rugosity was traced using a 'Wacom Intuos Pro' tablet (median size), and measured using Image J software. Results were averaged to give one rugosity value per bundle per donor.

Ligament insertion angles across the AM bundle were also measured. It was defined as the angle between the general direction of ligament proper (line of action) versus the approximate tangent of the cement line at the fibre bundle insertion point. A total of ten slices

were used for angle measurements for each sample. From the thirty labelled sections, starting from section number two, every third section was sampled to represent the span of sectioning across the medial to lateral most aspects. (i.e. sections 2, 5, 8, 11, 14, 17, 20, 23, 26, and 29). If a section was not capturing the full length of the ligament bundle insertion, the closest intact section was used instead. For the selection of measurement locations, the starting and ending points of the AM bundle on each section were defined before the distance in between was divided into 10 equidistant sections (9 full sections and 2 half sections). The 10 measurements were taken at the locations where the boundary lines of adjacent sections intercept with the cement line. For each section, the five measurements taken from the anterior part of the AM bundle were labelled as 'anterior' while the other five from the posterior aspect were labelled as 'posterior'. Thus, the AM bundle ligament angle measurements were divided into *four groups* according to their locations: Medial-Anterior, Medial-Posterior, Lateral-Anterior, and Lateral-Posterior. (Fig. 2) The results describe the ligament insertion angles across the AM bundle tibial enthesis. Measurements were then averaged to give one angle value per group per AM bundle.

All measurements were carried out by the lead author only to eliminate inter-rater reliability issue.

For imaging at the ultrastructural scale, scanning electron microscopy (SEM) was used. Preparation of the tissue structures followed our earlier protocol for porcine tissue (Zhao et al 2014) and involved hexane and ethanol treatment of the fixed and decalcified samples, and then critical point drying and coating before imaging.

RESULTS

At the macroscale, the double sub-bundle structure of the ACL, has been described in detail previously (Amis and Dawkins, 1991; Zantop et al., 2005; Petersen and Zantop, 2007). By contrast, at this same macroscale the AM and PL sub-bundles in the human ACL were not easily discernible (Fig. 1).

At the microscopic level, with sequential sectioning and beginning from the sagittal plane on the medial-most side, the PL region of the ACL begins to appear towards the parasagittal plane (Fig. 3- circled region). The contour of the ligament-bone junction also varied such that as it transits from the medial to the lateral aspect of the tibial plateau, it changes from having a wider attachment to a more focal one (Figs. 3 and 4 – see dotted lines). In the medial aspect of the AM region the ligament-proper direction is relatively orthogonal to the bone contour throughout the region, whereas in the posterior-lateral aspect of this AM region, the angle of the ligament line of action relative to the bone surface becomes more acute (Fig. 5).

Higher magnification views of the specific insertion morphologies revealed differences between the AM and PL regions. Ligament-to-bone interdigitation, with greater frequency and depth, would be structurally indicative of greater strength of attachment. The AM region showed extensive ligament-to-bone interdigitation and a highly irregular boundary between the bone and ligament fibres (Fig. 6). The tidemark, which separates the un-calcified and calcified fibrocartilaginous tissue, was also clearly visible in the AM bundle (Fig. 6C). In contrast, the insertion of the PL bundle displayed a relatively smooth boundary line at the ligament-to-bone interface with no visible tide mark (Fig. 6D). The insertion morphologies at the tibial enthesis were quantified using the rugosity index (Fig. 7). In spite of the small sample size, the average

rugosity index of the ligament-to-bone boundary line in the AM bundle was consistently larger than that of the PL bundle.

The larger rugosity values for the AM bundle were consistent with the intense interdigitation of this part of the ligament-bone insertion.

The bone insertion regions were explored further with SEM for both the AM (Fig. 8) and PL (Fig. 9) regions. The ligament fibrils of the AM region can be seen to be tightly bound within the bone fibrillar matrix via the interdigitations, these ending as 'pockets' of ligament fibrils 'packed' in bone matrix (Fig. 8). The PL region by contrast does not have this insertion morphology, and instead the fibrils end abruptly at the bone matrix interface (Fig. 9).

DISCUSSION

Few other studies have investigated the microstructure of the human ACL enthesis, especially in relation to the bundle regions. Arnoczky (1983) described the changes at the enthesis from ligament, fibrocartilage, and mineralized fibrocartilage, while more recently Beaulieu et al., (2015) quantified these changes. However, these studies did not distinguish between the AM and PL regions, nor did they describe the modes of attachment in relation to the bone, down to the ultrastructural and fibrillar scales, hence the relevance of this new study.

Starting with the macroscale, the difficulty in differentiating between the AM and PL bundles is consistent with the recent study by Smigielski et al., (2015) who found no clear separation of the AM and PL bundles of 111 human ACLs. It is important to note that this latter study involved only a macro-level structural analysis, and on this basis argued that instead of two bundles, the ACL formed a flat ribbon-like ligament from its femoral insertion to mid-substance.

However, there was little information in the Smigielski et al., study relating to the tibial insertion. Importantly, in the present study we have shown that at the bone attachment the insertion of the ACL into the tibia reveals a demarcation between two bundle groups (Fig. 3). In fact, the results suggest that the double bundle structure may be an intrinsic property of the ACL, and an earlier study by Ferretti et al., (2007) has found the two bundles can be clearly identified in human fetuses. Thus, any difficulty in discerning the two bundles may well be caused by developmental and age related structural changes, especially in our case, where the donors were all of advanced age. More of the implications regarding specimens from elderly people are included in the limitations section.

Based on the difference in microstructure at their points of insertion we argue that these two bundle groups are functionally distinct. The AM insertion region involves interdigitation while the PL does not. Deep interdigitation of the fibrocartilaginous zone into the bone tissue forms an irregular border between lamellar bone and calcified fibrocartilage (Cooper and Misol, 1970; Hurov, 1986; Gao et al., 1994). The shape of this interdigitation is said to be related to local loading conditions (Schneider, 1956). Gao and Messner (1996) mechanically loaded a range of rabbit knee ligaments, and found that greater *frequency* and *depth* of the interdigitations at the bone-soft tissue interface was positively correlated to the strength of the ligament. Skelley et al (2015), studying the human ACL showed that the AM bundle was significantly stronger than the PL bundle, but did not include an investigation of the insertions of the respective bundles into bone.

The interdigitation morphology, dominant in the AM region but much less so in the PL, is consistent with our earlier findings in the porcine ACL-bone junction (Zhao et al., 2014), and we suggest that this same morphological feature, now shown to be present in the human ACL,

contributes to strength of attachment, especially in relation to multiaxial loading (see Zhao et al., (2014), Fig. 12). We also suggest that the relatively smooth bone contour and shallow insertion of the PL region of the ACL, closer to the centre and sagittal midline of the joint, reflects its less dominant role in mechanical stabilisation. It has been suggested by microstructural property studies that the AM bundle is the primary load bearing region of the ACL with the AM bundle possessing a higher tissue modulus and failure to stress than the PL bundle (Skelley et al., 2015). The present study reinforces this point, where the difference in insertion morphology between the AM and PL region is consistent with the idea that the AM is more designed for larger loadings than the PL (Benjamin et al., 2006). Subsequently, such a differential loading configuration would be indicative that any excessive joint loading would translate more directly to the AM bundle than the PL. This difference in load bearing between the AM and PL regions may also help to explain why the AM bundle tends to be more commonly involved in partial ACL tears relative to the PL (Lorenz et al.; Ochi et al.; Zantop et al., 2007; Sonnery-Cottet et al., 2010; Chambat, 2013). However, it has also been shown that tears tend to occur near the femoral attachment (Zantop et al., 2007; Meyer et al., 2008). Thus conversely, it is possible that the strong AM bundle tibial insertion renders the femoral origin more prone to injuries. Moulton et al., (2017) have shown that the ACL femoral enthesis contains a mixture of indirect and direct insertions and Beaulieu et al., (2016) have found systematic reginal differences in collagen fibre attachment angles, however detailed microstructural characterization of the enthesis, especially data regarding to the interdigitation depth and frequency is still lacking. These counter arguments and knowledge gaps present scope for further investigation into the multi-scalar structural realties of the ACL in relation to its vulnerability to injury.

Of interest too is the change in bony contour of the AM region (Fig. 4), from the medial to the lateral aspect of the ACL insertion. Due to the small sample size and the descriptive nature of the study, the authors are careful to not make any conclusive inferences from this contour change. However, in an earlier study of the tibial enthesis of the ACL (Beaulieu et al 2015), while it was not inferred in that study, the contours displayed in the histology images (refer to Beaulieu et al 2015 Figures 3E and 3H) show very similar differences in bone contours from the medial most to lateral most aspects. The present authors therefore provide a hypothesis on the significance of such a contour change in the AM bundle in relation to the angle of insertion of the ligament, and the overall macro-level biomechanics of the ACL. The appearance of a relatively 'spread-out' insertion of fibres in the medial aspect relative to the lateral aspect where the insertion is more 'focal' in appearance (compare Fig. 4A with 4B) (Fig. 10) may be related to the function of the AM bundle. Studies have shown that the primary biomechanical role of the AM bundle is to resists anterior tibial translation (Kennedy et al., 1974; Norwood and Cross, 1979; Bach et al., 1997; Dienst et al., 2002; Amis, 2012). Further, the tibia being internally rotated relative to the femur during weight bearing (Markolf et al., 2014) would result in the anterior line of action coinciding with the lateral aspect of the AM region (Fig. 10B). A bone contour change from the AM medial to the AM lateral, may be to provide a more focally-directed AM bundle response when the tibia is relatively interior-rotated. In addition, a spreading out of the insertion in the medial aspect of the AM bundle, further from the knee center, would be beneficial in reducing stresses, and this idea is consistent with angles of insertion in this aspect of the bundle being relatively large, compared to the lateral aspect where they are more acute and directed towards the line of action (refer to e.g. Fig. 4B and 5).

Limitations. Several limitations to this study include the small sample size and the old age of the donors where all were greater than 85 years. ACL surgery is not performed on this patient population and the structural changes occurring with advanced aging could distort the microscopic anatomy of the ACL and be captured in study results. While further work will be required to include ACLs from a younger population, we believe that the data obtained from this study will still be applicable to improving our understanding of the multi-scalar transition of ligament morphology to its microstructural insertion into bone. In addition, the femoral insertion was not studied. However, the important findings from this study are that the attachment microstructural morphology at the ACL tibial enthesis varies regionally, and is consistent with the functional demands imposed on the ligament at the macro level.

The two ACL bundles were not easily discernible at the macroscopic level, and bony demarcations at the microscopic level were used to indirectly define the separation. Thus, there may be a possibility of misidentification of the boundary between the AM and the PL bundles. However, from the micro-images (Fig. 3), that the two bundles were correctly identified is supported by its morphological similarity to the porcine and ovine ACL split bundle structures that were studied earlier by the present authors (Zhao et al., 2014; Zhao et al., 2015). That the two bundles identified earlier in the porcine and ovine knee studies (Zhao et al., 2014; Zhao et al., 2015) were indeed the AM and PL bundles, is validated by the fact that in the animal ACLs, the anterior insertion of the lateral meniscus provides the gross separation of the two bundles (Proffen et al., 2012), helping to confirm that the microscale morphological differences in the ligament structure were indeed based on different bundle types. In the human ACL, there is no such gross separation by the lateral meniscal insertion, as this insertion is too laterally positioned (Proffen et al., 2012). However, the similarity at the microscale in the ligament morphology

between the animal and human ACLs provides confidence that the AM and PL bundles identified in the present study are correct.

Quantitative analyses have been carried out by measuring the rugosity values between bundles and the ligament attachment angles between regions of the AM bundle. Although the averaged results in both measurements show a consistent trend, no definite conclusions based on statistical analysis can be made on the quantitative differences of this small sample size.

The present study also shows that the human attachments between the two bundle-types are very similar to those seen previously in the porcine ACL where the AM bundle insertion displayed stronger interdigitation, with the PL bundle comprising a more gradual blending of the soft tissue and bone (Zhao et al., 2014). The important insight is that this study shows the need for further exploration into the enthuses of the ACL, especially across scalar-levels.

In terms of a clinical significance, despite the above limitations, this data from this study suggests that the multi-scale structure, as well as the insertion morphology of the ACL is highly complex, which may further imply that current double bundle reconstruction strategies should take into consideration these complexities. More consideration towards the different sub-bundle alignments and insertion morphologies may be needed in order to further improve the outcomes of ACL reconstruction surgeries.

REFERENCES

Amis AA. 2012. The functions of the fibre bundles of the anterior cruciate ligament in anterior drawer, rotational laxity and the pivot shift. Knee surgery, sports traumatology, arthroscopy : official journal of the ESSKA 20:613-620.

Amis AA, Dawkins GPC. 1991. Functional anatomy of the anterior cruciate ligament. The Journal of Bone and Joint Surgery 73-B:8.

Arnoczky SP. 1983. Anatomy of the anterior cruciate ligament. Clinical orthopaedics and related research 172:19-25.

Bach JM, Hull ML, Patterson HA. 1997. Direct measurement of strain in the posterolateral bundle of the anterior cruciate ligament. Journal of Biomechanics 30:281-283.

Beaulieu ML, Carey GE, Schlecht SH, Wojtys EM, Ashton-Miller JA. 2015. Quantitative comparison of the microscopic anatomy of the human ACL femoral and tibial entheses. Journal of Orthopaedic Research 33:1811-1817.

Beaulieu ML, Carey GE, Schlecht SH, Wojtys EM, Ashton-Miller JA. 2016. On the heterogeneity of the femoral enthesis of the human ACL: microscopic anatomy and clinical implications. Journal of Experimental Orthopaedics 3:14.

Benjamin M, Toumi H, Ralphs JR, Bydder G, Best TM, Milz S. 2006. Where tendons and ligaments meet bone: attachment.. Journal of anatomy:20.

Chambat P. 2013. ACL tear. Orthopaedics & traumatology, surgery & research : OTSR 99:S43-52.

Cooper RR, Misol S. 1970. Tendon and ligament insertion. Journal of Bone and Joint Surgery 52-AQ:21.

Dai C, Guo L, Yang L, Wu Y, Gou J, Li B. 2015. Regional fibrocartilage variations in human anterior cruciate ligament tibial insertion: a histological three-dimensional reconstruction. Connective tissue research 56:18-24.

Dai X. 2012. Anatomic double-bundle anterior cruciate ligament reconstruction. Chinese Journal of Traumatology 15:175-179.

Dienst M, Burks RT, Greis PE. 2002. Anatomy and biomechanics of the anterior cruciate ligament. Orthopedic Clinics of North America 33:605-620.

Ferretti M, Doca D, Ingham SM, Cohen M, Fu FH. 2012. Bony and soft tissue landmarks of the ACL tibial insertion site: an anatomical study. Knee Surgery 20:62-68.

Ferretti M, Levicoff EA, Macpherson TA, Moreland MS, Cohen M, Fu FH. 2007. The fetal anterior cruciate ligament: an anatomic and histologic study. Arthroscopy : the journal of arthroscopic & related surgery : official publication of the Arthroscopy Association of North America and the International Arthroscopy Association 23:278-283.

Fu RZ, Lin DD. 2013. Surgical and biomechanical perspectives on osteoarthritis and the ACL deficient knee: a critical review of the literature. The Open Orthopaedics Journal 7:292-300.

Gadikota HR, Hosseini A, Asnis P, Li G. 2015. Kinematic Analysis of Five Different Anterior Cruciate Ligament Reconstruction Techniques. Knee Surg Relat Res 27:69-75.

Gao J, Messner K. 1996. Quantitative comparison of soft tissue-bone interface at chondral ligament insertions in the rabbit knee joint. Journal of anatomy 188:7.

Gao J, Oqvist G, Messner K. 1994. The attachement of the rabbit medial meniscus. a morphological investigation using image analysis and immunohistochemistry. Journal of anatomy 185:5.

Harner CD, Baek GH, Vogrin TM, Carlin GJ, Kashiwaguchi S, Woo SL. 1999. Quantitative analysis of human cruciate ligament insertions. Arthroscopy : the journal of arthroscopic & related surgery : official publication of the Arthroscopy Association of North America and the International Arthroscopy Association 15:741-749.

Hofbauer M, Muller B, Wolf M, Forsythe B, Fu FH. 2013. Anatomic Double-Bundle Anterior Cruciate Ligament Reconstruction. Operative Techniques in Sports Medicine 21:47-54.

Hurov JR. 1986. Soft-tissue bone interface: how do attachments of muscles, tendons, and ligaments change during growth? a light microscopic study. Journal of Morphology:13.

Kato Y, Hoshino Y, Ingham SJ, Fu FH. 2010. Anatomic double-bundle anterior cruciate ligament reconstruction. J Orthop Sci 15:269-276.

Kennedy JC, Weinberg HW, Wilson AS. 1974. The anatomy and function of the anterior cruciate ligament. The Journal of Bone and Joint Surgery 56-A:223-235.

Lorenz S, Illingworth KD, Fu FH. Diagnosis of Isolated Posterolateral Bundle Tears of the Anterior Cruciate Ligament. Arthroscopy : the journal of arthroscopic & related surgery : official publication of the Arthroscopy Association of North America and the International Arthroscopy Association 25:1203-1204.

Markolf KL, Jackson SR, Foster B, McAllister DR. 2014. ACL forces and knee kinematics produced by axial tibial compression during a passive flexion-extension cycle. Journal of orthopaedic research : official publication of the Orthopaedic Research Society 32:89-95.

Meyer EG, Baumer TG, Slade JM, Smith WE, Haut RC. 2008. Tibiofemoral contact pressures and osteochondral microtrauma during anterior cruciate ligament rupture due to excessive compressive loading and internal torque of the human knee. The American journal of sports medicine 36:1966-1977.

Moffat KL, Sun WH, Pena PE, Chahine NO, Doty SB, Ateshian GA, Hung CT, Lu HH. 2008. Characterization of the structure-function relationship at the ligament-to-bone interface. Proceedings of the National Academy of Sciences of the United States of America 105:7947-7952.

Moulton SG, Steineman BD, Haut Donahue TL, Fontbote CA, Cram TR, LaPrade RF. 2017. Direct versus indirect ACL femoral attachment fibres and their implications on ACL graft placement. Knee surgery, sports traumatology, arthroscopy : official journal of the ESSKA 25:165-171.

Norwood LA, Cross MJ. 1979. Anterior cruciate ligament: functional anatomy of its bundles in rotatory instabilities. The American Journal of Sport Medicine 7:23-26.

Ochi M, Adachi N, Uchio Y, Deie M, Kumahashi N, Ishikawa M, Sera S. A Minimum 2-Year Follow-up After Selective Anteromedial or Posterolateral Bundle Anterior Cruciate Ligament Reconstruction. Arthroscopy : the journal of arthroscopic & related surgery : official publication of the Arthroscopy Association of North America and the International Arthroscopy Association 25:117-122.

Petersen W, Zantop T. 2007. Anatomy of the anterior cruciate ligament with regard to its two bundles. Clinical orthopaedics and related research 454:35-47.

Proffen BL, McElfresh M, Fleming BC, Murray MM. 2012. A comparative anatomical study of the human knee and six animal species. The Knee 19:493-499.

Schneider H. 1956. Zur struktur der sehnenansatzzonen. Zeitschrift fur Anatomie und Entwicklungsgeschichte 119:431-456.

Skelley NW, Castile RM, York TE, Gruev V, Lake SP, Brophy RH. 2015. Differences in the microstructural properties of the anteromedial and posterolateral bundles of the anterior cruciate ligament. The American journal of sports medicine 43:928-936.

Smigielski R, Zdanowicz U, Drwiega M, Ciszek B, Ciszkowska-Lyson B, Siebold R. 2015. Ribbon like appearance of the midsubstance fibres of the anterior cruciate ligament close to its femoral insertion site: a cadaveric study including 111 knees. Knee surgery, sports traumatology, arthroscopy : official journal of the ESSKA 23:3143-3150.

Sonnery-Cottet B, Lavoie F, Ogassawara R, Scussiato RG, Kidder JF, Chambat P. 2010. Selective anteromedial bundle reconstruction in partial ACL tears: a series of 36 patients with mean 24 months follow-up. Knee Surgery 18:47-51.

Steineman BD, Moulton SG, Haut Donahue TL, Fontbote CA, LaPrade CM, Cram TR, Dean CS, LaPrade RF. 2016. Overlap Between Anterior Cruciate Ligament and Anterolateral Meniscal Root Insertions: A Scanning Electron Microscopy Study. The American journal of sports medicine.

Yasuda K, Tanabe Y, Kondo E, Kitamura N, Tohyama H. 2010. Anatomic double-bundle anterior cruciate ligament reconstruction. Arthroscopy : the journal of arthroscopic & related surgery : official publication of the Arthroscopy Association of North America and the International Arthroscopy Association 26:S21-34.

Zantop T, Herbort M, Raschke MJ, Fu FH, Petersen W. 2007. The role of the anteromedial and posterolateral bundles of the anterior cruciate ligament in anterior tibial translation and internal rotation. Ameracan Journal of Sports Medicine 35:223-227.

Zantop T, Petersen W, Fu FH. 2005. Anatomy of the anterior cruciate ligament. Operative Techniques in Orthopaedics 15:20-28.

Zhao L, Thambyah A, Broom ND. 2014. A multi-scale structural study of the porcine anterior cruciate ligament tibial enthesis. Journal of anatomy 224:624-633.

Zhao L, Thambyah A, Broom N. 2015. Crimp morphology in the ovine anterior cruciate ligament. Journal of anatomy 226:278-288.

FIGURE LEGENDS

Figure 1: Macro-scale images showing the difficulty in discerning the sub-bundle morphology. In (A) the two bundles are discerned by palpation and the two dotted arrows indicate the sub-bundles. (B) A sagittal plane image indicating the AM bundle (dotted arrow) and PL region (approximately outlined) later confirmed in microscopic imaging.

Figure 2: selection of angle measurement locations. Ten measurements were made at equidistance on each section (red circles). The five measurements from the anterior aspect (in green region) of the bundle were labelled as 'Anterior' and the other five from the posterior aspect (in blue region) were labelled as 'Posterior'.

Figure 3. From serial sectioning in the sagittal plane, the following three images are displayed: (A) Medial-most plane showing only the AM region, (B) approximately parasagittal plane showing the start of the PL bundle (black dotted circle), and (C) relative lateral aspect showing how the entire ACL is approximately divided equally into the two sub-bundle types. The dotted white lines in B and C outline the change in the bone contour of the AM region. The black arrow points to a bone-demarcation between the two sub bundles.

Figure 4: AM region (A) medial and(B) lateral aspects relative to the parasagittal plane. The dashed lines show the approximate tibia plateau and associated bone contours. The white arrows indicate the relative line of action of the AM bundle. (C) and (D) are medial and lateral aspects of the AM insertion of another sample, showing some difference but in essence the same change in contours.

Figure 5: Averaged ligament angle measurements in the AM bundle. Angles in the lateral-posterior aspect were consistently smaller than those from the rest of the AM bundle.

Figure 6: Comparison of the enthesis morphology between the (A) & (C) AM and the (B) & (D) PL bundles at different magnifications. The AM bundle displayed a deeper interdigitation and a more irregular bone contour (white dash lines) than the PL bundle. The AM bundle also had a clearly visible tide mark as indicated by the white arrow.

Figure 7: Averaged rugosity measurements. Values from the AM bundles were consistently larger than those from the PL bundles.

Figure 8. AM-bundle region. A series of images with increasing magnification showing the ultimate junction morphology of the ligament and bone tissue. (A) DIC image in which the dotted box outlines the end of an interdigitation of ligament tissue into bone. (B) SEM image of that shown in A. (C) DIC image, higher magnification, of the dotted box region in A. (D) SEM image of that shown in C. (E) and (F) Increasing magnification in SEM of region X shown in D. (G) and (H) Increasing magnification in SEM of region Y shown in D. Note the 'pocket' like insertion of the ACL into bone (as outlined).

Figure 9. PL-bundle region. A series of images with increasing magnification showing the ultimate junction morphology of the ligament and bone tissue. (A) DIC image in which the dotted box outlines the junction of ligament tissue into bone. (B) SEM image of that shown in A. (C) DIC image, higher magnification, of the dotted box region in A. (D) SEM image of that shown in C. (E) and (F) Increasing magnification in SEM of the junction (dotted box). (G) and (H) Increasing magnification in SEM of regions X and Y shown in F. Note the abrupt ends of

the ACL fibrils in (G) and the occasional bundle of ligament fibrils (black arrow) that extend beyond.

Figure 10. The transverse view of the tibial plateau shows that in load bearing the tibia is relatively inward rotated and an approximate line of action (black arrow) depicts anterior tibial translation. The representative 'footprint' of the ACL and its sub-bundles (AM and PL) is also outlined in the transverse view schematic. The two black lines on the footprint represent the sagittal plane imaging reported in this study. Plane A represents the relative medial aspect of the ACL and plane B the lateral. (A) Schematic of the AM-bundle bone contour in plane A. (B) Schematic of the AM-bundle bone contour in plane B.

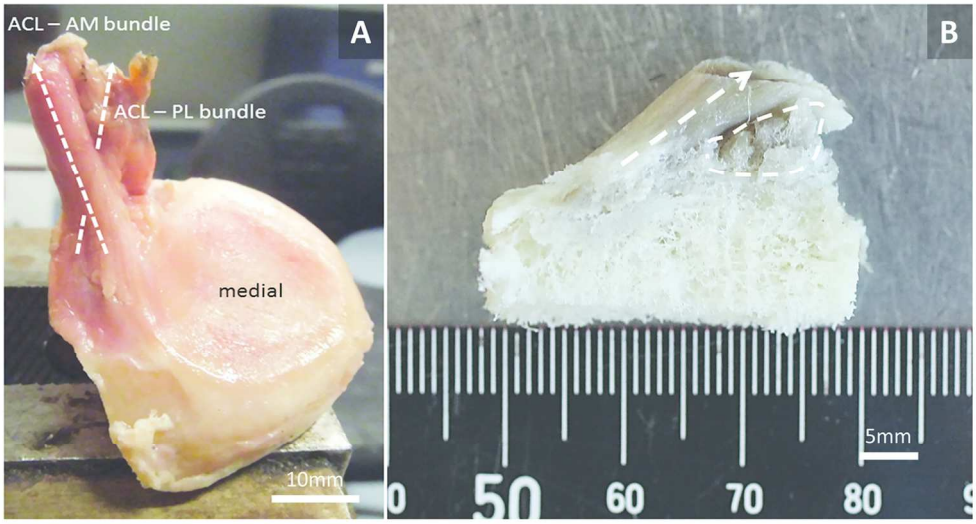

Figure 1: Macro-scale images showing the difficulty in discerning the sub-bundle morphology. In (A) the two bundles are discerned by palpation and the two dotted arrows indicate the sub-bundles. (B) A sagittal plane image indicating the AM bundle (dotted arrow) and PL region (approximately outlined) later confirmed in microscopic imaging.

117x64mm (300 x 300 DPI)

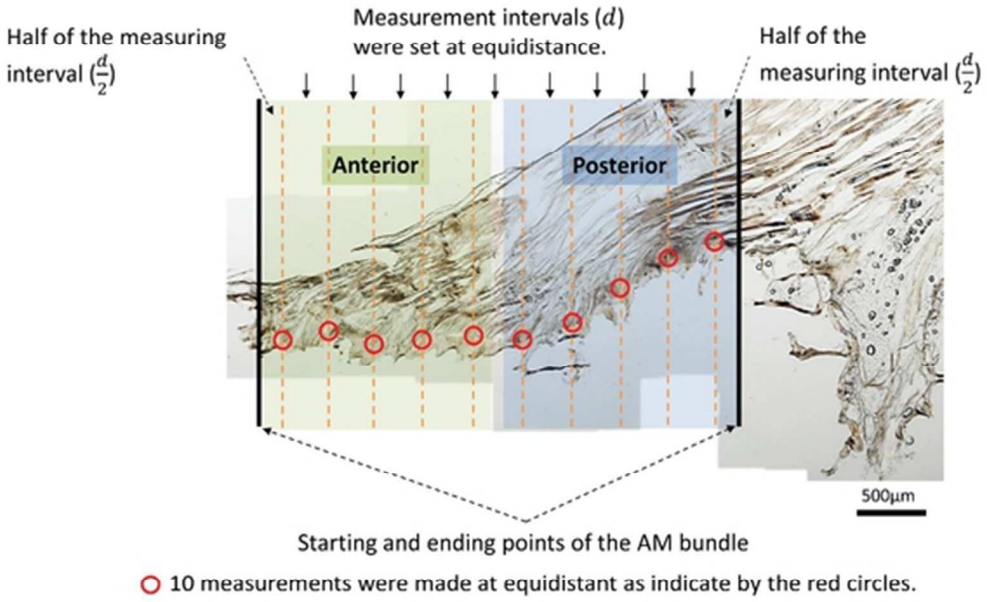

Figure 2: selection of angle measurement locations. Ten measurements were made at equidistance on each section (red circles). The five measurements from the anterior aspect (in green region) of the bundle were labelled as 'Anterior' and the other five from the posterior aspect (in blue region) were labelled as 'Posterior'.

48x36mm (300 x 300 DPI)

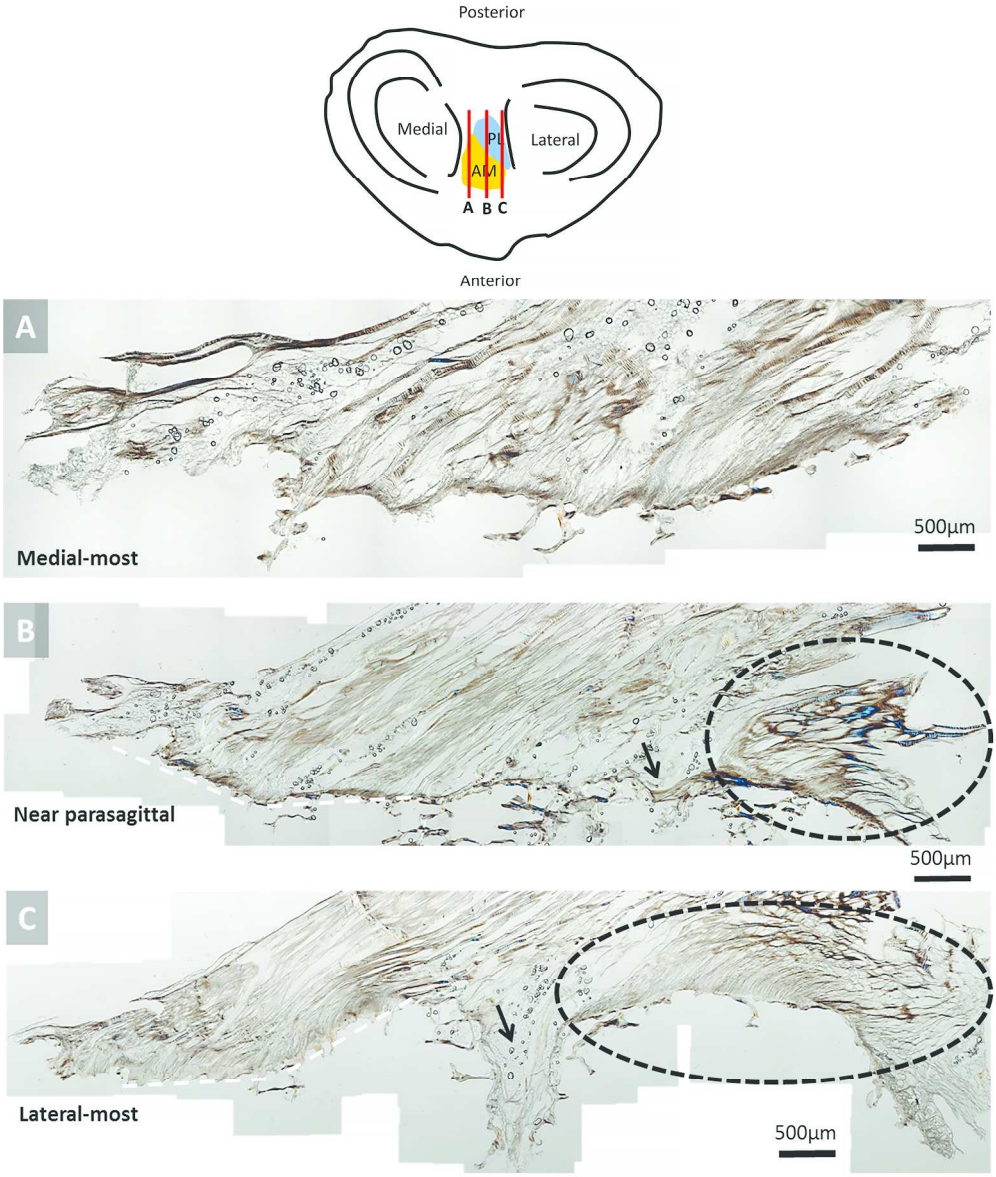

Figure 3: From serial sectioning in the sagittal plane, the following three images are displayed: (A) Medial-most plane showing only the AM region, (B) approximately parasagittal plane showing the start of the PL bundle (black dotted circle), and (C) relative lateral aspect showing how the entire ACL is approximately divided equally into the two sub-bundle types. The dotted white lines in B and C outline the change in the bone contour of the AM region. The black arrow points to a bone-demarcation between the two sub bundles.

230x279mm (300 x 300 DPI)

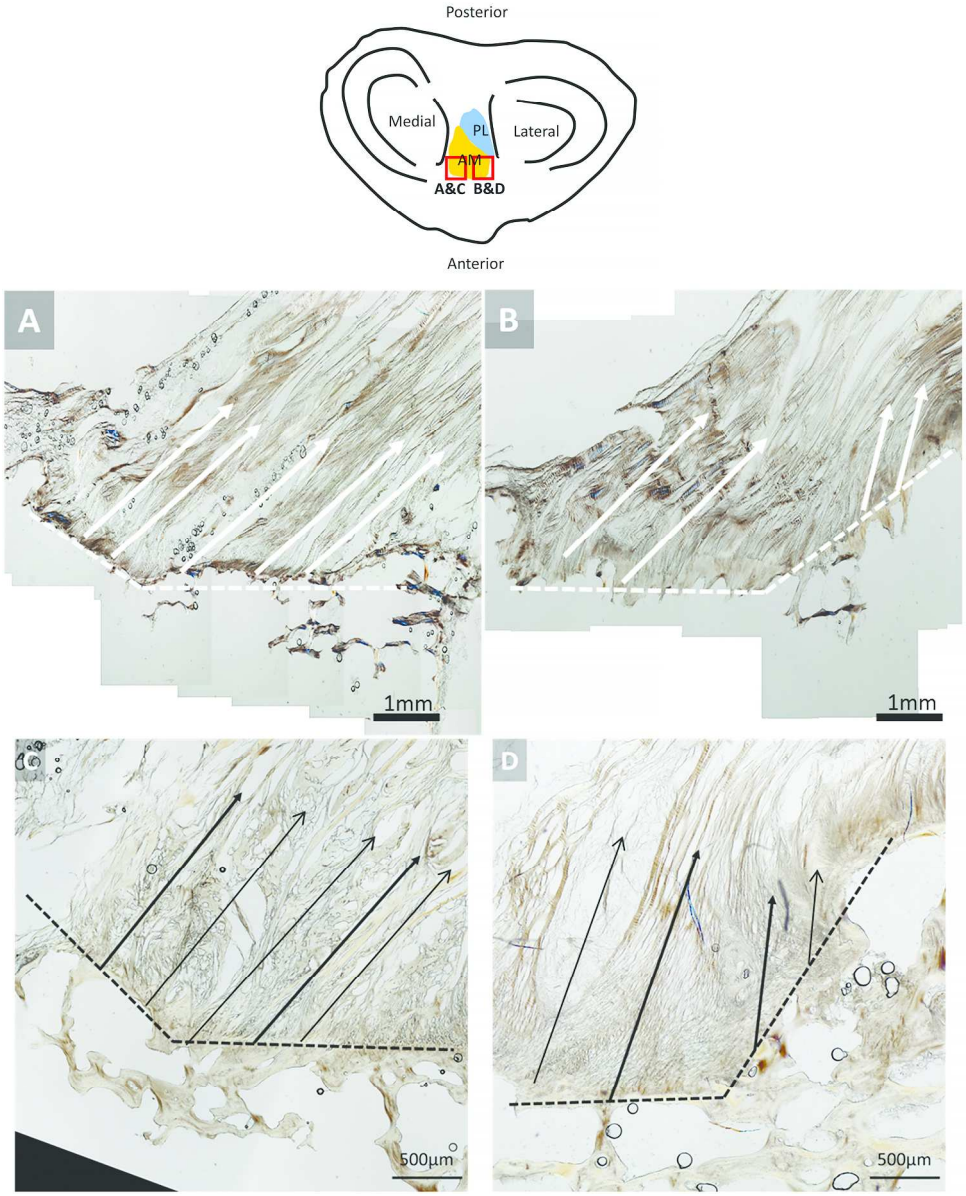

Figure 4: AM region (A) medial and(B) lateral aspects relative to the parasagittal plane. The dashed lines show the approximate tibia plateau and associated bone contours. The white arrows indicate the relative line of action of the AM bundle. (C) and (D) are medial and lateral aspects of the AM insertion of another sample, showing some difference but in essence the same change in contours.‼ ┼

237x296mm (300 x 300 DPI)

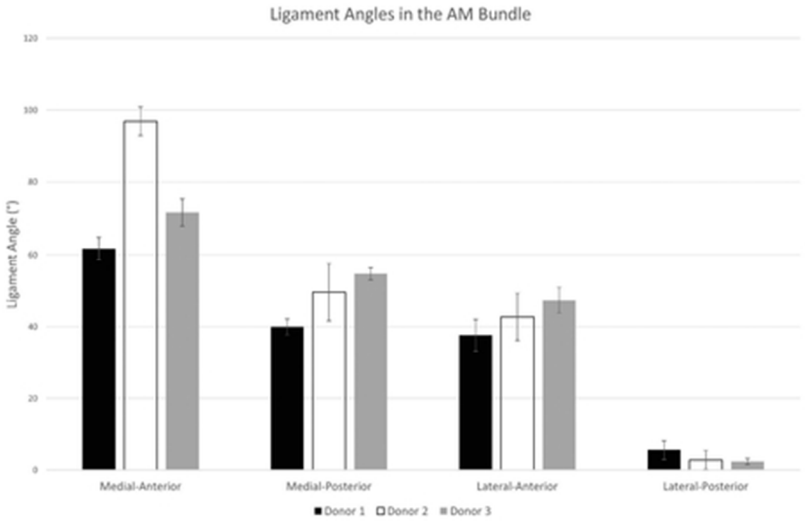

Figure 5: Averaged ligament angle measurements in the AM bundle. Angles in the lateral-posterior aspect were consistently smaller than those from the rest of the AM bundle.

48x27mm (300 x 300 DPI)

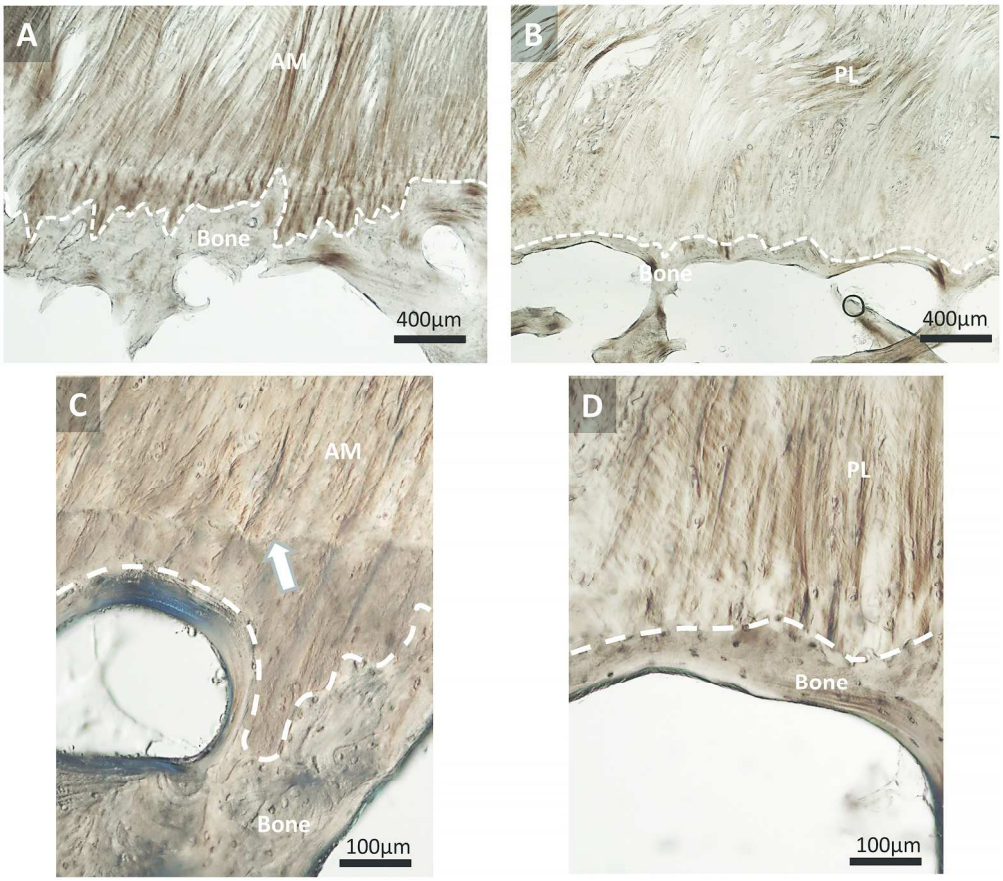

Figure 6: Comparison of the enthesis morphology between the (A) & (C) AM and the (B) & (D) PL bundles at different magnifications. The AM bundle displayed a deeper interdigitation and a more irregular bone contour (white dash lines) than the PL bundle. The AM bundle also had a clearly visible tide mark as indicated by the white arrow.

183x161mm (300 x 300 DPI)

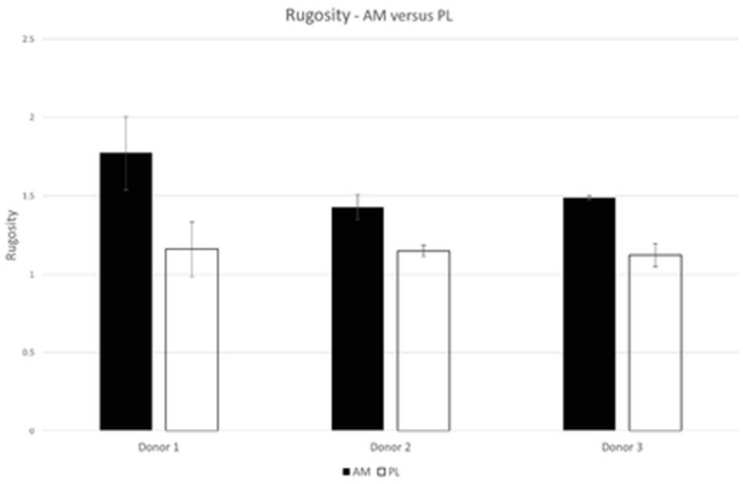

Figure 7: Averaged rugosity measurements. Values from the AM bundles were consistently larger than those from the PL bundles.

48x27mm (300 x 300 DPI)

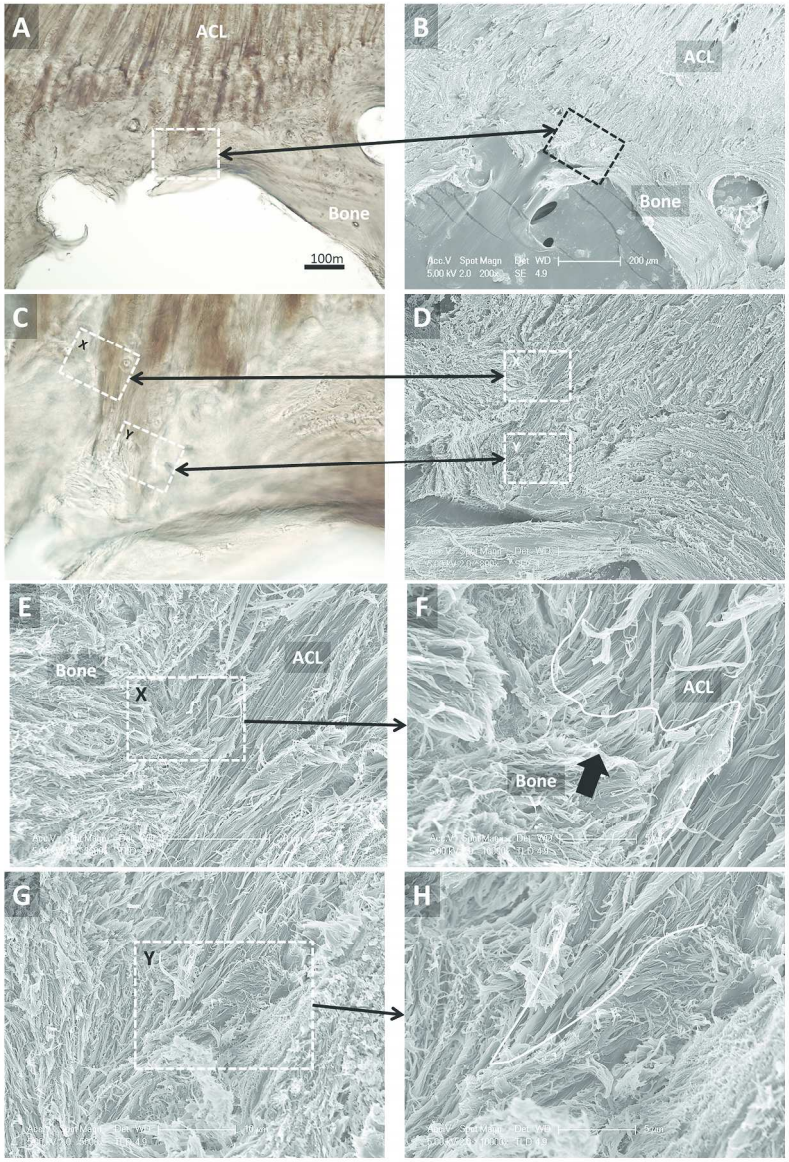

Figure 8: AM-bundle region. A series of images with increasing magnification showing the ultimate junction morphology of the ligament and bone tissue. (A) DIC image in which the dotted box outlines the end of an interdigitation of ligament tissue into bone. (B) SEM image of that shown in A. (C) DIC image, higher magnification, of the dotted box region in A. (D) SEM image of that shown in C. (E) and (F) Increasing magnification in SEM of region X shown in D. (G) and (H) Increasing magnification in SEM of region Y shown in D. Note the 'pocket' like insertion of the ACL into bone (as outlined).

280x409mm (300 x 300 DPI)

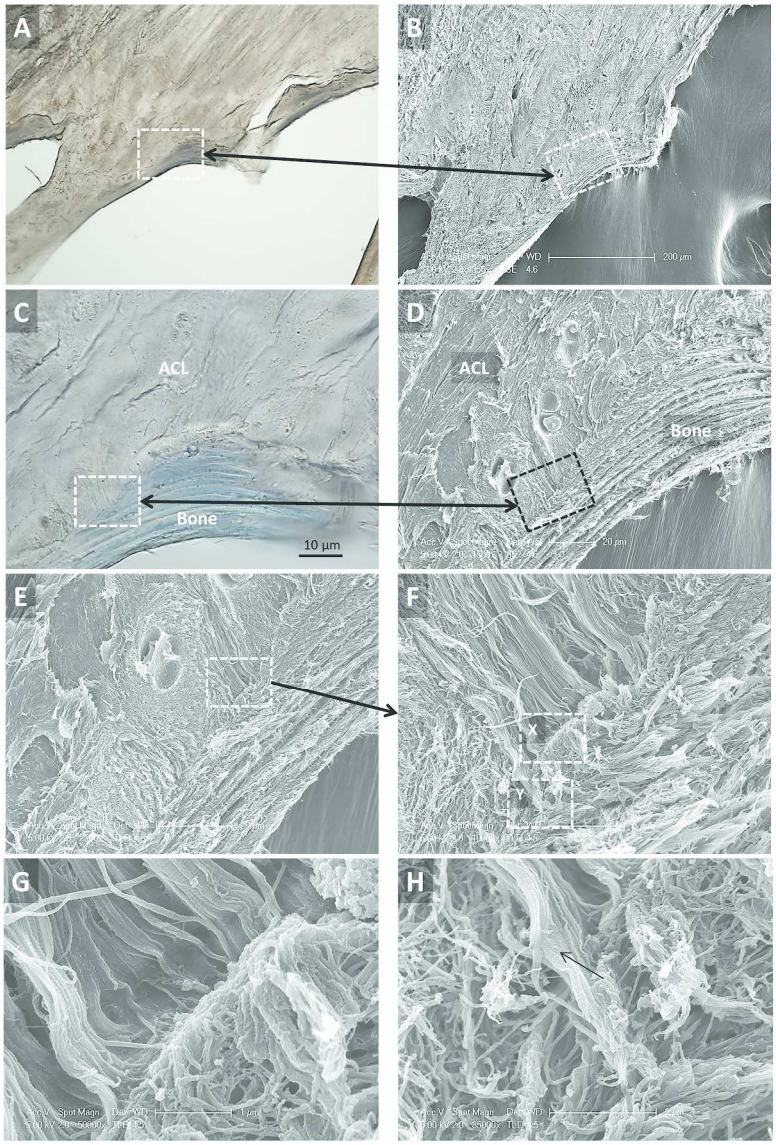

Figure 9: PL-bundle region. A series of images with increasing magnification showing the ultimate junction morphology of the ligament and bone tissue. (A) DIC image in which the dotted box outlines the junction of ligament tissue into bone. (B) SEM image of that shown in A. (C) DIC image, higher magnification, of the dotted box region in A. (D) SEM image of that shown in C. (E) and (F) Increasing magnification in SEM of the junction (dotted box). (G) and (H) Increasing magnification in SEM of regions X and Y shown in F. Note the abrupt ends of the ACL fibrils in (G) and the occasional bundle of ligament fibrils (black arrow) that extend beyond.

273x394mm (300 x 300 DPI)

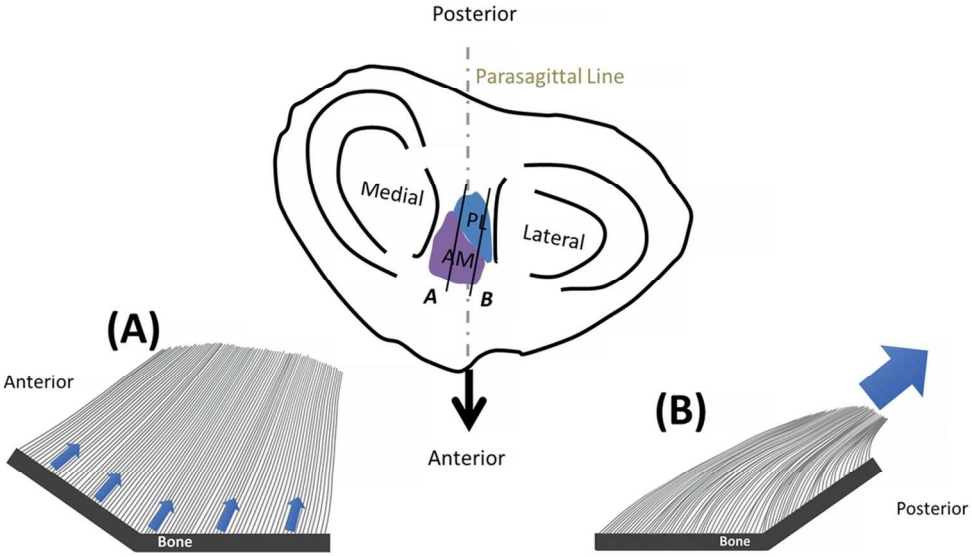

Figure 10: The transverse view of the tibial plateau shows that in load bearing the tibia is relatively inward rotated and an approximate line of action (black arrow) depicts anterior tibial translation. The representative 'footprint' of the ACL and its sub-bundles (AM and PL) is also outlined in the transverse view schematic. The two black lines on the footprint represent the sagittal plane imaging reported in this study. Plane A represents the relative medial aspect of the ACL and plane B the lateral. (A) Schematic of the AM-bundle bone contour in plane A. (B) Schematic of the AM-bundle bone contour in plane B.

97x55mm (300 x 300 DPI)